SINGLE FOLDING ANALYSIS OF THE ELASTIC SCATTERING OF p-^{16}O

E.H. Esmael, M.A. Allam†

Physics Department, Faculty of Science, Cairo University
12613 Giza, Egypt

(Received July 21, 2006; revised version received December 6, 2006; final version received May 20, 2007)

The elastic scattering of p-^{16}O data at different proton incident energies have been analyzed using single-folding model. In the present calculations analytical expressions for the real part of the optical potential are derived by folding different sets of nucleon–nucleon (NN) interactions to different forms of densities of the target nucleus. The theoretical calculations of the differential cross sections as well as analyzing power gave a reasonable fit to that of the experimental data.

PACS numbers: 24.10.Ht, 25.40.Cm, 27.20.+n

1. Introduction

Elastic scattering of nucleon–nucleus data at intermediate energies are useful tools for testing and analyzing nuclear structure models and intermediate energy reaction theories [1–10]. The elastic scattering of proton–nucleus has been analyzed in order to determine ground state matter densities empirically for comparison with Hartree–Fock predictions [11–13]. The study of spin dependent effect at the intermediate energy proton scattering plays an important role. At such region of energy, polarization data has rich structure, that is closely related to diffraction structure in the corresponding elastic scattering process [2, 14].

The optical potential has been extensively used in studying the proton–nucleus scattering [15]. It was suggested by Elton [16] that the optical potential for proton–nucleus at medium energies differs in shape from the customarily used Woods–Saxon (WS) form. The elastic scattering calculations for ^{12}C and ^{16}O gave the same conclusion [17–20]. As the particle energies exceed 100 MeV, the potential becomes less attractive in the nuclear interior than near the nuclear surface.

† mallam50@yahoo.com

There have been several relativistic treatments of proton–nucleus elastic scattering [21–25]. The Glauber multiple scattering theory and eikonal approximation have been also used to analyze the intermediate energy proton–nucleus elastic scattering data [26–28]. Crespo *et al.* [19] used corrections to the first order term of multiple scattering expression of nucleon–nucleus optical potential in order to describe nucleon scattering on ^{16}O and ^{208}Pb target nuclei at 100 MeV, 200 MeV and 400 MeV incident energies. Besides a relativistic description of elastic scattering nucleon–nucleus data, there are also microscopic non-relativistic scattering theories for describing such data [29–31]. The phenomenological optical model (WS) was used to analyze the elastic nucleon–nucleus scattering in the same region of energy [17–20].

In the present work, the analytical single folding model is used to describe both the elastic differential cross section and the analyzing power of proton scattering on ^{16}O at 135 MeV and 200 MeV incident energies. In the present calculations, the considered folding potential is derived by folding the target density with two different models of the effective NN-interaction. In Section 2 we introduce the formulation of the used optical potentials. Results and discussion are given in Section 3, while the conclusion is given in Section 4.

2. Formalism

The real part of the optical potential for the nucleon–nucleus elastic scattering is given for the single folding model, in the following form [32]

$$U_F(\bar{R}) = \int d\bar{r}_1 \rho_1(\bar{r}_1) V(\bar{r})\,, \tag{1}$$

where $\bar{r} = \bar{R} - \bar{r}_1$, $\rho_1(\bar{r}_1)$ is the matter density distribution of the target nucleus, $V(\bar{r})$ is the effective NN-interaction.

In the present calculation the effective NN-interaction is taken according to Knyzakov and Hefter [33] and has three forms. The first one consists of a single Gaussian term and is denoted by F_1.The second consists of two Gaussian terms and is denoted by F_2. The last one consists of two Gaussian terms plus a zero range exchange term which is denoted by F_3. The general form of such an interaction is given as

$$V(\bar{r}) = \sum_{k=1}^{3} V_k e^{-r^2/a_k^2} + d(E)\delta(\bar{r})\,, \tag{2}$$

where $d(E)$ is given in Table I.

The parameters of the above NN-interaction are given in Table I.

TABLE I

Parameters for the NN-interaction.

Set	V_1 (MeV)	V_2 (MeV)	a_1 (fm)	a_2 (fm)	$d(E)$ fm^{-3} MeV
F_1	-20.97	—	1.47	—	—
F_2	-553.18	1781.4	0.8	0.5	—
F_3	-601.99	2256.4	0.8	0.5	$-276(1.0005)E/A$

The density of the ^{16}O target nucleus is considered in three forms. First is the modified Gaussian form [34] (MGM) given as

$$\rho_1(r_1) = \rho_0 \left[e^{-r_1^2/b_0^2} + c_2 \left(\frac{r_1}{b_2}\right)^2 e^{-r_1^2/b_2^2} \right] , \tag{3}$$

where ρ_0, c_2, b_0 and b_2 are constant parameters, and their values are given in Table II.

TABLE II

Density parameters for the MGM (Model 1).

ρ_0 (fm^{-3})	b_0 (fm)	b_2 (fm)	c_2
0.125	1.99	1.75	1.77

The second form is the simple alpha cluster model [35] (SACM). Following Wadia [35], the spherical part of the density of ^{16}O can be written as

$$\rho_1(r_1) = \left(\frac{1}{b\sqrt{\pi}}\right)^3 \sqrt{\frac{\pi}{2t}} I_{1/2}(t) e^{-\left(r_1^2+R_1^2\right)/b^2} , \tag{4}$$

where $t = 2R_1 r_1/b^2$, $I_{1/2}(t)$ is the modified Bessel function of the order of $1/2$. R_1 is the distance of the alpha cluster from the center of the nucleus, b is the size parameter which is related to cluster radius a_k by $a_k^2 = \frac{3}{2}b^2$.

The third form is the Brink's alpha cluster model (BACM). According to Brink [36] and Hassan *et al.* [37], the spherical part of the density of ^{16}O, in its ground state, can be written as

$$\begin{aligned} \rho_1(r_1) = & \frac{e^{-\left(r_1^2+R_1^2\right)/b^2}\sqrt{r_1}}{4\left(b\sqrt{\pi}\right)^3(1+3\eta)(1-\eta)} \\ & \times \left[4(1+2\eta)\sqrt{\frac{\pi b^2}{4R_1}} I_{1/2}(t) - 12\eta \sqrt{\frac{\pi b^2\sqrt{3}}{4R_1}} I_{1/2}(t) \left(\frac{t}{\sqrt{3}}\right) \right] , \end{aligned} \tag{5}$$

where $\eta = e^{\frac{2}{3}\gamma^2}$, $\gamma = \frac{R_1}{b}$, $t = 2R_1 r_1/b^2$.

The parameters for SACM and BACM models are given in Table III.

TABLE III

Parameters for SACM (Model 2) and BACM (Model 3).

SACM (Model 2)		BACM (Model 3)	
b (fm)	R_1 (fm)	b (fm)	R_1 (fm)
1.34	1.98	1.6	1.46

The analytical form of the real part of the optical potential is obtained by substituting Eqs. (2)–(5) into Eq. (1) and carrying out the required integrations over r_1. The total optical potential is considered with four different methods. In the first method, the optical potential is given by

$$V_{\mathrm{OP}}(r) = N_F U_F(r) + iW_I F_I(r) + \lambda_\pi^2 [V_{\mathrm{SO}} g_{\mathrm{VSO}}(r) + iW_{\mathrm{SO}} g_{\mathrm{WSO}}(r)](\bar{L}\bar{\sigma})\,, \quad (6)$$

where

$$\begin{aligned} g_j(r) &= \frac{1}{r}\frac{d}{dr}[1 + e^{(r - r_j A_T^{1/3})/a_j}]^{-1}\,, \\ F_I(r) &= [1 + e^{(r - r_j A_T^{1/3})/a_I}]^{-1}\,, \\ \lambda_\pi^2 &= \left(\frac{h}{m_\pi c}\right)^2 . \end{aligned}$$

The second method is expressed as:

$$V_{\mathrm{OP}}(r) = (N_F + iN_I) U_F(r) + \lambda_\pi^2 [V_{\mathrm{SO}} g_{\mathrm{VSO}}(r) + iW_{\mathrm{SO}}(r) g_{\mathrm{WSO}}(r)](\bar{L}\bar{\sigma})\,. \quad (7)$$

In the third method the potential takes the form:

$$V_{\mathrm{OP}}(r) = N_F U_F(r) + iW_I F_I(r) + U_{\mathrm{LS}}(r)\,, \quad (8)$$

with

$$U_{\mathrm{LS}}(r) = C_{\mathrm{LSG}} g_{\mathrm{MSO}}(r)(\bar{L}\bar{\sigma})\,, \qquad g_{\mathrm{MSO}} = \frac{1}{r}\frac{d}{dr}\rho r\,,$$

and

$$\begin{aligned} \rho(r) &= 0.19\left[1 + e^{2r - 9.4}\right]^{-1} - 0.052\left[1 + e^{3.23r - 2.58}\right]^{-1}\,, \\ C_{\mathrm{LSG}} &= \lambda_\pi^2 (V_{\mathrm{SO}} + iW_{\mathrm{SO}})\ \left(\mathrm{fm}^3\right) . \end{aligned}$$

In the last method it is given in the following form:

$$V_{\mathrm{OP}}(r) = (N_F + iN_I) U_F(r) + U_{\mathrm{LS}}(r)\,. \quad (9)$$

3. Results and discussion

The experimental data of both elastic scattering differential cross section and analyzing power of scattering for proton on ^{16}O at 135 MeV and 200 MeV incident energies [20,39] have been analyzed using single folding model. The numerical calculations have been done using the DWUCK4 [38] code. In the present calculations, we have derived different analytical expressions for the real part of the optical potential in the frame of single folding model. These expressions are obtained by folding the general form of the NN-interaction expressed by Eq. (2), with the three forms of the densities of the target nucleus ^{16}O given by Eqs. (3), (4) and (5). These expressions are obtained by substituting the target densities and the NN-interaction in Eq. (1) and carrying out the necessary integrations over r_1. In our derivations we have used three different sets of parameters, denoted by F_1, F_2 and F_3, for the effective NN-interactions in its general form of Eq. (2). The parameters of the three sets are given in Table II. The density of the ^{16}O target nucleus is contained in three forms as indicated by Eqs. (3),(4), and (5).

Fig. 1 displays the behavior of the real part of the optical model considered for the three suggested models of the target nuclear densities and their variation with the different sets of the NN-interactions. It is clear from Fig. 1(a) that the strength of the real part at small distances is less for models 1 and 2 than that for model 3. The same behavior is observed for the other two sets F_2 and F_3 as shown in Fig. 1(b) and (c), respectively. Fig. 1(d) displays the real part for model 1 of the assumed optical potentials for the different three sets of the NN-interactions. It is clear from Fig. 1(d) that the real part of the potential at small distances is smaller for F_1 than that for the other two sets.

The best fit between the present theoretical calculations of both differential cross section and analyzing power with the experimental data is obtained with F_1 (least central depth and largest dispersion) of NN-interaction potential rather than the other two sets (as shown in Fig. 2). This behavior is verified for both of 135 MeV and 200 MeV incident energies and for the different methods stated in the theory which is a natural behavior due to the trend of the real part of the optical potentials displayed in Fig. 1(d).

In the present calculations, the total optical potential is considered with four different methods. In the first one, the real part of the optical potential is the single folding model, while both imaginary and spin-orbit terms are chosen in the form of phenomenological Woods–Saxon form (WS) as given by Eq. (6). The parameters for this method at 135 MeV and 200 MeV incident energies are given in Table IV.

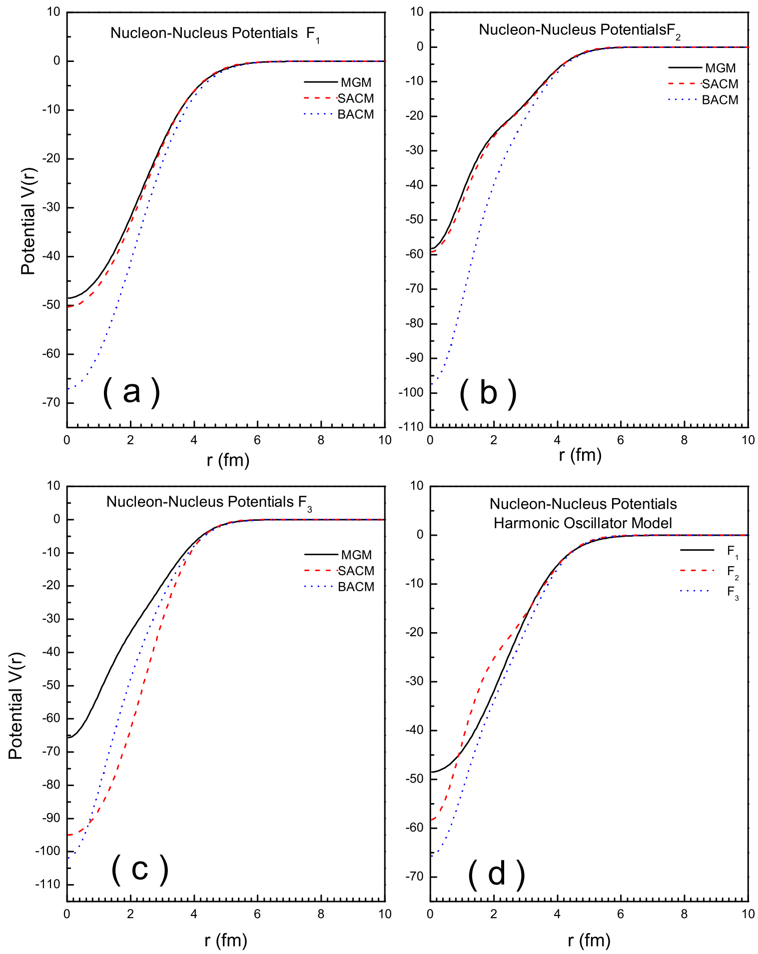

Fig. 1. Radial distribution for the real part of the optical potentials for each set of NN-interactions with the different models (a), (b), and (c) for model 1 with the three NN-sets. The solid, dotted, and dashed curves, respectively, represent the optical potentials for the MGM, SACM, and BACM. In panel (d) the curves represent the three sets of NN-interactions with the MGSM.

The calculations with such a method for both elastic scattering differential cross section and analyzing power for the two energies considered are shown in Fig. 3(a) and (b), respectively. From Fig. 3(a) there is a satisfactory fit between the theoretical calculation and the experimental data for the differential cross section for models 1 and 2 of the target densities rather than model 3. In the case of 135 MeV incident energy, it is shown in Fig. 3(a) that the fit of the experimental data [39] for the analyzing power

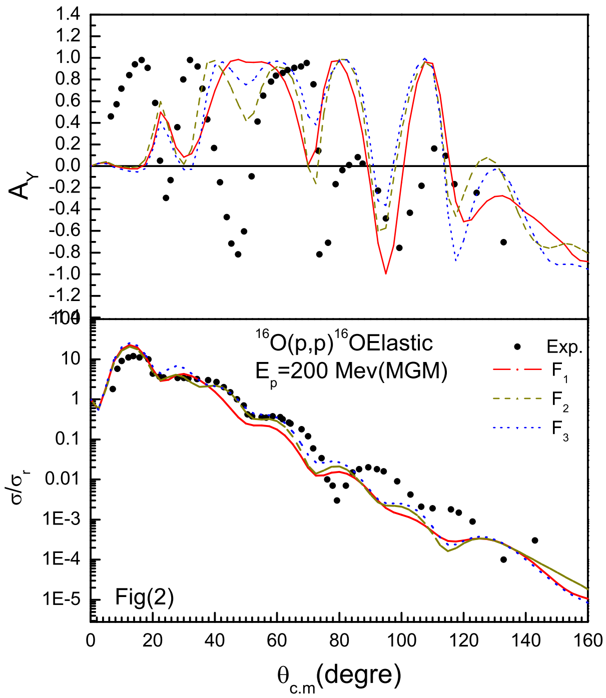

Fig. 2. Ratio of the elastic scattering cross section to the Rutherford cross section σ/σ_R and analyzing power A_Y, are plotted *versus* the center of mass momentum scattering angle calculated with method 1 for different sets of NN-interaction at 200 MeV.

is worse than that obtained for the elastic differential cross section. In the case of 200 MeV incident energy, there is a satisfactory fit of the differential cross section experimental data for the three considered models of the target densities except in the range scattering angles between 70° and 120°.

In the second method of calculation the imaginary part of the optical potential is taken as a part of the real folding term through the normalization constant N_I. But the spin-orbit term is a phenomenological WS form. The optical model parameters for this method at 135 MeV and 200 MeV incident energies are given in Table V.

The fitting of the experimental data is shown in Fig. 4(a) and (b). It is clear from Fig. 4(a) that there is less improvement in the fitting of the experimental data for model 1 of the target density relative to that obtained with other method 1. But for two other models of the densities of the target nucleus the agreement with the experimental data specially in the range of scattering angles between 26° and 38° is worse. In the case of the analyzing power, there is a slight improvement of the fit to the experimental data for

TABLE IV

Optical model parameters used in method (1).

Opt. model parameters	135 MeV Model 1	Model 2	Model 3	200 MeV Model 1	Model 2	Model 3
N_F	0.95	0.95	0.95	0.8	0.8	0.8
N_I	—	—	—	—	—	—
W_I MeV	−25.02	−25.02	−25.02	−24.1	−24.5	−27.5
r_1 (fm)	1.182	1.182	1.182	1.03	1.03	1.03
a_I (fm)	0.773	0.773	0.773	0.678	0.678	0.678
$V_{\rm SO}$ MeV	−3.48	−3.48	−3.48	−6.1	−5.6	−5.3
$W_{\rm SO}$ MeV	2.26	2.26	2.26	4.7	5.2	4.4
$r_{\rm VSO}$ (fm)	0.92	0.92	0.92	0.88	0.88	0.88
$a_{\rm VSO}$ (fm)	0.506	0.506	0.506	0.625	0.625	0.625
$r_{\rm WSO}$ (fm)	0.92	0.92	0.92	0.942	0.942	0.942
$a_{\rm WSO}$ (fm)	0.506	0.506	0.506	0.49	0.49	0.49
$\xi^2(\sigma)$	9048.4	9046.7	9041.5	5457.2	5255.3	5625.9
$\xi^2(A_Y)$	15331	15328	15319	9246.2	8904.1	9532.1
$\sigma_{\rm R}$ mb	310.6	311	314.3	235.91	237.41	257.53
$\sigma_{\rm tot}$ mb	502.9	503.4	508.4	325.3	327.37	355.11

TABLE V

Optical model parameters used in method (2).

Opt. model parameters	135 MeV Model 1	Model 2	Model 3	200 MeV Model 1	Model 2	Model 3
N_F	0.95	0.95	0.95	0.8	0.8	0.8
N_I	0.9	0.9	0.9	0.7	0.7	0.7
$V_{\rm SO}$ MeV	−4.48	−4.48	−4.48	−8.644	−8.644	−8.644
$W_{\rm SO}$ MeV	2.26	2.26	2.26	6.512	6.512	6.512
$r_{\rm VSO}$ (fm)	0.92	0.92	0.92	0.88	0.88	0.88
$a_{\rm VSO}$ (fm)	0.506	0.506	0.506	0.625	0.625	0.625
$r_{\rm WSO}$ (fm)	0.92	0.92	0.92	0.942	0.942	0.942
$a_{\rm WSO}$ (fm)	0.506	0.506	0.506	0.49	0.49	0.49
$\xi^2(\sigma)$	9039.4	9033.1	9070.2	5336.5	5318.6	5567.5
$\xi^2(A_Y)$	15314	15304	15367	9042	9010	9434
$\sigma_{\rm R}$ mb	291.7	286.9	381.5	256.9	257.2	266.5
$\sigma_{\rm tot}$ mb	472.3	464.5	526.0	354.21	354.57	367.43

model 3 of the target density. From Fig. 4(b) there is some improvement in the agreement with the experimental data specially in the range of scattering angles 80° to 120°. But for the analyzing power the fit is worse than that obtained with method 1.

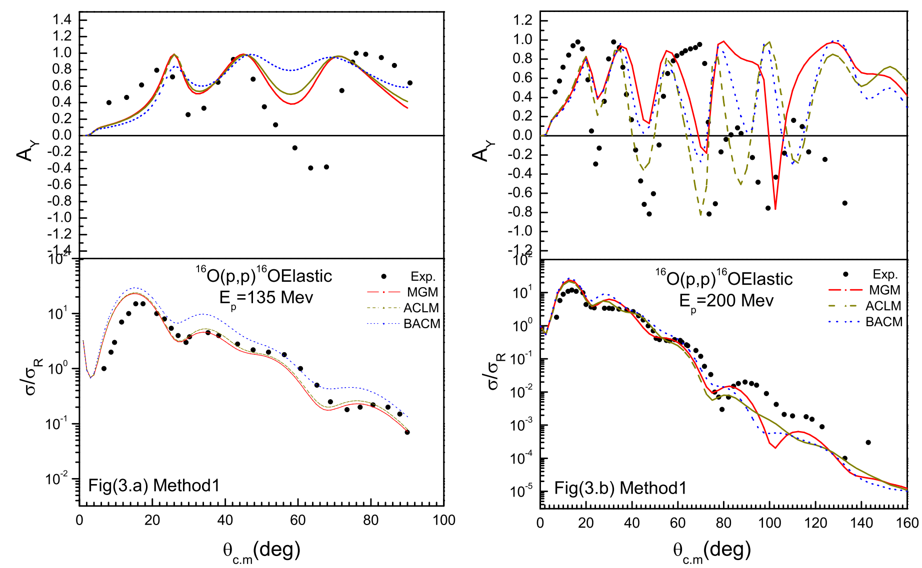

Fig. 3. Ratio of the elastic scattering cross section to the Rutherford cross section, $\sigma/\sigma_{\rm R}$, and analyzing power, A_Y, plotted *versus* the center of mass momentum scattering angle as calculated with method 1 for set 1 at 135 MeV (Fig. 3(a)), and at 200 MeV (Fig. 3(b)) proton incident energies using the parameters given in Table IV. The solid, dotted and dashed curves, respectively, represent the three models MGM, SACM and BACM, while the black circles represent experimental data.

In the third method both real and spin-orbit parts of the optical potential are considered in microscopic form given in Eq. (7). The optical model parameters for such method at 135 MeV and 200 MeV incident energies are given in Table VI. The resulting fit to the data is displayed in Fig. 5(a) and 5(b). It can be seen from Fig. 5(a) that there is some improvement of the fit to the experimental data for the target density model 3, unlike for the other two models. It is clear from Fig. 5(b) that there is some improvement relative to methods 1 and 2 in the agreement with the experimental data for both differential cross section and analyzing power, specially in the range of scattering angles less than 80°.

In the last method 4, all parts of the optical potential are taken to be of the microscopic form (Eq. (9)). The calculations are shown in Figs 6(a) and (b). The optical model parameters for this method at 135 MeV and 200 MeV incident energies are given in Table VII.

It could be noticed from Fig. 6(a) that there is some improvement of the fit to the experimental data for both differential cross section and analyzing power compared with that obtained by the previous three methods. In the

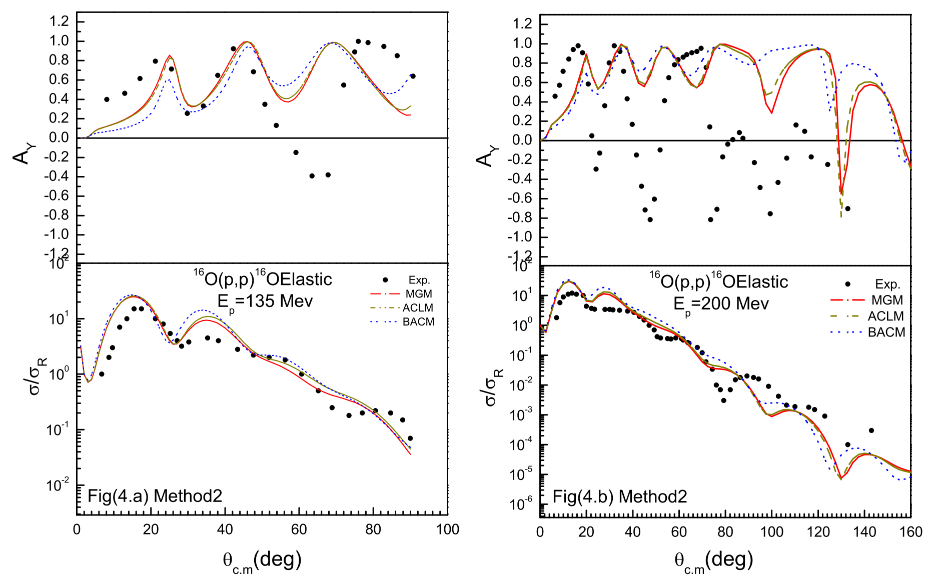

Fig. 4. The same as Fig. 3 except that the calculations are performed with the method 2 and parameters given in Table V.

TABLE VI

Optical model parameters used in method (3).

Opt. model parameters	135 MeV Model 1	135 MeV Model 2	135 MeV Model 3	200 MeV Model 1	200 MeV Model 2	200 MeV Model 3
N_F	0.95	0.95	0.95	0.8	0.8	0.8
N_I	—	—	—	—	—	—
W_I MeV	−26.02	−26.02	−26.02	−24.7	−27.3	−29.12
r_I (fm)	1.182	1.182	1.182	1.03	1.03	1.03
a_I (fm)	0.773	0.773	0.773	0.678	0.678	0.678
V_{SO} MeV	−18.48	−18.48	−18.48	−7.945	−7.626	−7.505
W_{SO} MeV	16.26	16.26	16.26	6.669	6.384	6.343
$\xi^2(\sigma)$	9059.4	9057.4	9053.8	2513.8	3526.2	3954.5
$\xi^2(A_Y)$	15350	15349	15347	4259.2	5974.5	6700.2
σ_{R} mb	312.4	313.1	315.5	239.1	254.9	266.6
σ_{tot} mb	505.8	506.1	510.8	329.01	351.51	367.7

case of 200 MeV incident energy, Fig. 6(b), we can notice that there is an extremely good fit to the experimental data for differential cross section at scattering angles greater than 70°. The analyzing power shows relative improvement compared to the previous three methods and all types of densities of the target nuclei.

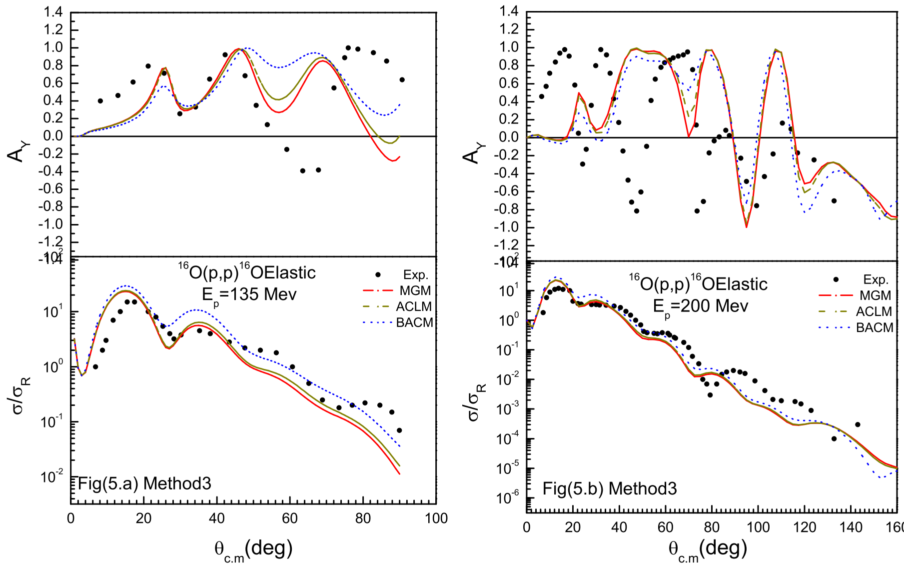

Fig. 5. The same as Fig. 3 except that the calculations are performed with the method 3 and parameters given in Table VI.

TABLE VII

Optical model parameters used in method (4).

Opt. model parameters	135 MeV Model 1	Model 2	Model 3	200 MeV Model 1	Model 2	Model 3
N_F	0.95	0.95	0.95	0.72	0.71	0.699
N_I	0.75	0.75	0.75	0.593	0.595	0.588
$V_{\rm SO}$ MeV	−18.48	−18.48	−18.48	−8.717	−8.607	−8.574
$W_{\rm SO}$ MeV	16.26	16.26	16.26	6.669	6. 813	6.731
$\xi^2(\sigma)$	9041.8	9035.3	9062.8	3002.2	3293.5	3785.1
$\xi^2(A_Y)$	16319.6	15308.7	15355.7	5086.3	5580.2	6413.2
$\sigma_{\rm R}$ mb	298.5	306.1	317.9	250.6	255.6	274.5
$\sigma_{\rm tot}$ mb	483.3	495.5	514.7	345.5	352.4	378.5

In the case of elastic scattering of protons on ^{16}O at 135 MeV the present results using method 1 give a reasonable fit to the experimental data for both differential cross section and analyzing power, which is comparable with that obtained by Amos *et al.* [39, 45] except at scattering angles less than 20°. Model 1 gives a comparable fit for both elastic scattering differential cross section and analyzing power as that obtained by Kelly *et al.* [40] using impulse calculations. But the present calculations give a comparable fit for the differential cross section calculated using local density approximation by

Kelly *et al.* [40] and less satisfactory fit for the analyzing power calculations. The non-relativistic full folding model calculation [41] gives less satisfactory fit to the experimental data for both differential cross section and analyzing power than that obtained with the present models. But the present calculations give some better agreement with the experimental data for both differential cross section and analyzing power compared to that obtained by full folding model considered by Arellano *et al.* [42].

The present calculation for both differential cross section and analyzing power at energy of 200 MeV obtained with the fourth method gives a comparable fit for angles greater than 120° with that obtained by Glover *et al.* [20] for phenomenological double WS real and imaginary parts of the optical potential and both the phenomenological and macroscopic spin-orbit term of the potential. Meanwhile, our calculations are better than that obtained by Glover *et al.* [20] using single WS optical potential for angles greater than 85°. The microscopic relativistic calculations of Murdock and Horowitz [25] gave worse fit to2 the experimental data than obtained with the present model calculations. Full folding optical model potentials give a comparable fit to the experimental data for differential cross section as the present model. But for the analyzing power, the present calculation gives better fit than that obtained by Elster *et al.* [43]. The same conclusion is reached when comparing our calculations with those using non-relativistic full folding model made by Arellano *et al.* [41] as well as the relativistic Brueckner–Hartree model calculations made by both Chen and Mackellar [8], which are more accurate and give a better fit than the non-relativistic calculations. The same conclusion is reached for the case of microscopic calculations of medium effects considered by Sammarruca *et al.* [9].

4. Conclusion

From the above results and discussion we reach the following conclusions. The present single folding model gives a reasonable fit to the experimental data for both differential cross section and analyzing power at 135 MeV and 200 MeV incident energy. The set F_1 of NN-interaction gives the best description of both differential cross section and analyzing power. The microscopic form of the real, imaginary and spin-orbit terms of the optical potential gives a better description of the experimental data of the considered reaction than the WS forms of all parts of the optical potential. In order to reach definite conclusion, the same model should be applied to wider range of energies and other types of target nuclei. The disagreement between the theoretical models and the experimental data can be reduced by the application of the density dependent [44] effect in the NN-interaction.

REFERENCES

[1] H.O. Mayer, P. Schwandt, G.L. Moake, P.P. Singh, *Phys. Rev.* **C23**, 616 (1981).

[2] M. Jaminon, C. Mahaux, P. Rochus, *Phys. Rev.* **C22**, 2027 (1980).

[3] C. Mahaux, *Lect. Notes Phys.* **89**, 1 (1979).

[4] F.A. Brieva, J.R. Rook, *Nucl. Phys.* **A297**, 299 (1977); *Nucl. Phys.* **A291**, 317 (1977); *Nucl. Phys.* **A297**, 206 (1978); *Nucl. Phys.* **A307**, 493 (1978).

[5] L. Ray *et al.*, *Phys. Rev.* **C23**, 828 (1981).

[6] R.D. Amado, J.A. McNeil,, D.A Sparrow, *Phys. Rev.* **C23**, 2186 (1981).

[7] M. Rashan, *Eur. Phys. J.* **A16**, 371 (2003).

[8] B.Q. Chen, A.D. Mackellar, *Phys. Rev.* **C52**, 878 (1995).

[9] F. Sammarruca, E.J. Stephenson, K. Jiang, *Phys. Rev.* **C60**, 064610 (1999).

[10] R. Crespo, R.C. Johnson, J.A. Tostevin, *Phys. Rev.* **C53**, 3022 (1996).

[11] L. Ray, G.W. Hoffmann, W.R. Coker, *Phys. Rep.* **212**, 223 (1992).

[12] L. Ray, *Phys. Rev.* **C19**, 1856 (1979); *Phys. Rev.* **C20**, 1857 (1979).

[13] L. Ray, G.W. Hoffmann, R.M. Thalar, *Phys. Rev.* **C22**, 1454 (1980).

[14] G.W. Hoffmann *et al.*, *Phys. Rev.* **C21**, 1488 (1980).

[15] R.D. Amado, J.A. McNeil, D.A. Sparrow, *Phys. Rev.* **C23**, 2114 (1981).

[16] L.R.B. Elton, *Nucl. Phys.* **89**, 89 (1966).

[17] H.O. Mayer, P. Schwandt, W.W. Jacobs, J.R. Hall, *Phys. Rev.* **C27**, 459 (1983).

[18] H.O. Mayer, P. Schwandt, G.L. Moake, P.P. Singh, *Phys. Rev.* **C23**, 616 (1981).

[19] H.O. Mayer, J.Hall, W.W. Jacobes, P. Schwandt, P.P. Sigh, *Phys. Rev.* **C24**, 1782 (1981).

[20] C.W. Glover *et al.*, *Phys. Rev.* **C31**, 1 (1985).

[21] C. Mahuax, *AIP Conf. Proc.* **97**, 20 (1983); H.V. Von Geramb, *AIP Conf. Proc.* **97**, 44 (1983).

[22] B.C. Clark, S. Hama, R.L. Mercer, *Phys. Rev.* **C23**, 260 (1981).

[23] J.A. McNeil, J.R. Shepand, S.J. Wallac, *Phys. Rev. Lett.* **50**, 1443 (1983).

[24] J.A. Tjon, S.J. Wallac, *Phys. Rev.* **C32** , 1667 (1985).

[25] D.P. Murdock, C.J. Horowitz, *Phys. Rev.* **C35**, 1442 (1987).

[26] I.M.A. Tag Eldin, E.H. Esmael, M.Y.M. Hassan, M.N.H. Comsan, *J. Phys. G Nucl. Part. Phys.* **17**, 271 (1991).

[27] C.A. Bertulani, H. Sagawo, *Nucl. Phys.* **A588**, 667 (1995).

[28] J.S. Khalili, J.A. Tostesvin, I.J. Thompson, *Phys. Rev.* **C54**, 1843 (1996).

[29] E. Boridy, H. Feshbach, *Ann. Phys. (NY)* **109**, 468 (1977).

[30] K.L. Kowalski, *Nucl. Phys.* **A416**, 465C (1984).

[31] K. Amos *et al.*, *Adv. Nucl. Phys.* **25**, 275 (2000).

[32] G.R. Satchler, W.G. Love, *Phys. Rev.* **C55**, 183 (1979).

[33] O.H. Knyarkov, E.F. Hefter, *Z. Phys.* **A301**, 277 (1981).

[34] V.V. Burov, O.M. Knyazkov, A.A. Shirokava, K.V. Shitikova, *Z. Phys.* **A313**, 319 (1983).

[35] W. Wadia, M.K.H. Hegab, *Atomker Atomkernenrgie (ATKE)* **Bd.26**, 269 (1975).

[36] D.M. Brink *et al.*, *Phys. Lett.* **33B**, 143 (1971).

[37] M.Y.M. Hassan, W. Wadia, International Center for Theoretical Physics, Trieste, Italy 1977, Ic/72/125.

[38] P.D. Kunz, E. Rost, in *Computational Nuclear Physics 2*, eds. K. Langanke *et al.*, Springer-Verlag, Berlin 1993, p. 88; N.M. Clarke, Hi-Optim 94.2 Code, University of Birmingham, 1994.

[39] K. Amos *et al.*, *Nucl. Phys.* **A413**, 225 (1984).

[40] J.J. Kelly *et al.*, *Phys. Rev.* **C39**, 1222 (1989).

[41] H.F. Arellano, F.A. Breiva, W.G. Love, *Phys. Rev.* **C41**, 2188 (1990).

[42] H.F. Arellano, W.G. Love, F.A. Breiva, *Phys. Rev.* **C43**, 2743 (1991).

[43] Ch. Elster, T. Cheon, E.F. Redish, P.C. Tandy, *Phys. Rev.* **C41**, 814 (1990).

[44] D. Gupta, E. Khan, Y. Blumenfeld, *Nucl. Phys.* **A773**, 230 (2006); A.K. Charadhri, *Nucl. Phys.* **A449**, 243 (1986).

[45] K. Amos, S. Karataglidis, Y.J. Kim, *Nucl. Phys.* **A762**, 230 (2005).